Carbon Nanotube-Supported Copper-Cobalt Catalyst for the Production of Higher Carbon Number Alcohols through Carbon Monoxide Hydrogenation

Peng Wang,[a] Xihua Du,*,[a] Wenchang Zhuang,[a] Keying Cai,[a] Jing Li,[a] Yan Xu,[a] Yingmei Zhou,[a] Kai Sun,[b] Shuyao Chen,[b] Xiaoli Li[b] and Yisheng Tan*,[b]

[a]School of Chemistry and Chemical Engineering, Xuzhou Institute of Technology, 221018 Xuzhou, China

[b]State Key Laboratory of Coal Conversion, Institute of Coal Chemistry, Chinese Academy of Sciences, 030001 Taiyuan, China

A series of carbon nanotube (CNTs)-supported copper-cobalt catalysts were prepared and investigated in a slurry reactor for their ability to selectively convert syngas into higher carbon number alcohols. The 7.5Cu7.5Co/CNTs catalyst achieved superior selectivity towards the formation of ethanol (30.1%) and C_{2+} alcohols (57.7%), while the 10Co5Cu/CNTs catalyst exhibited the largest alcohol space-time yield (372.9 mg g_{cat}^{-1} h^{-1}). However, the pure Cu (15Cu/CNTs) catalyst displayed negligible activity. Cobalt reduction was enhanced in the presence of copper. In addition to the Cu^0–Co^0 center, Co^0–Co^{2+} also presented dual active sites for higher alcohols synthesis, the Co^{2+} site could terminate carbon chain growth to produce alcohols. The ratio of Cu/Co considerably influences the metal particle properties-synergistically effecting the active species.

Keywords: CO hydrogenation, higher alcohols synthesis, CuCo, carbon nanotube

Introduction

The conversion of synthesis gas derived from coal, natural gas or biomass into higher carbon number alcohols is both attractive and challenging to the field of C1 chemistry.[1-3] The alcohols obtained from this process can be used as fuel blends or as value-added chemicals in fine chemical synthesis.[4,5] Furthermore, higher alcohols synthesis (HAS) is a prototypical example of reactions that rely on synergistic effects between dual catalytic sites with different functionalities, one active site catalysis CO dissociation, while the second site enables CO non-dissociation centers to form.[6] Typically, among the available non-precious metal catalysts, modified bimetallic Fischer-Tropsch (FT) catalysts (e.g., CuCo) are widely investigated as one of the most promising candidates for HAS.[7,8]

Therefore, synergistic combination of two metals represents an efficient approach towards desirable catalytic properties by the creation of hybrid sites, and intimate contact between the metal components has been recognized as important to achieve satisfactory selectivity. It is known that Co species are the center for CO dissociation, hydrogenation and chain propagation to form surface alkyl species, while Cu species are the site for molecularly absorbed CO insertion and alcohol formation.[9,10] The synergistic effect and the surface distribution of the two active components have significant influence on the catalytic performance for the synthesis of alcohols.[11,12] It has been demonstrated that the porous structure of the support may efficiently control metal dispersion.[13,14] For supported catalysts, metal particle size is typically limited by the pore size of the support and the support texture may prevent sintering of the metal particles[15] or limit sintering to the maximum pore diameter.[16,17] Furthermore, it is expected that the nature of the support may influence copper-cobalt interactions, which may lead to different active phase structures and properties. SiO_2, Al_2O_3 and TiO_2 have different interactions with cobalt species. Strongly interacting supports such as γ-Al_2O_3 usually lead to high cobalt oxide dispersions, however, there is difficulty to reduce cobalt species.[18] To obtain appropriate Cu and Co nanoparticle properties and distribution in the catalyst, carbon nanotubes (CNTs) are employed as supports. A wealth of interdependent research[19-21] has demonstrated the advantages of using CNTs as supports

*e-mail: 12dxh@sina.com; tan@sxicc.ac.cn

to improve transition metal particle dispersion in catalysts and the confinement effects during catalysis have been systematically studied. Previous studies concluded that space restriction,[22] enrichment of reactants inside CNTs[23] and the electronic interaction of the confined materials within CNTs[24] is expected to facilitate cobaltous oxide reduction. Therefore, there is a need to minimize the distance between dual catalytic sites, while maintaining active particles of sufficiently small size with a high degree of dispersion induced by the confinement effects of nanotubes.

In the present study, a series of CNTs-supported CuCo-based precursors with different Cu/Co ratios were synthesized using a simple and effective co-impregnation method. After calcination, a homogeneous and highly dispersed bimetallic catalyst was obtained, as revealed by high-resolution transmission electron microscopy (HRTEM) analysis. *In situ* X-ray photoelectron spectroscopy (XPS) indicated Cu^0–Co^0 and Co^0–Co^{2+} centers were the active sites for HAS in our system. The catalytic performance of the catalysts prepared in this work towards the hydrogenation of carbon monoxide was examined in a slurry reactor. The maximum space-time yield (STY) reached 372.9 mg g_{cat}^{-1} h^{-1} and an ethanol selectivity as high as 30.1% was obtained. Improved synergistic effects were observed between the dual active sites at a Cu/Co ratio range of 0.5-2, with the ratio exerting significant influence on the catalytic performance.

Experimental

Materials

Analytical-grade chemicals, including $Cu(NO_3)_2 \cdot 3H_2O$ and $Co(NO_3)_2 \cdot 6H_2O$ were purchased from the Beijing Chemical Co., Ltd. and were used as received without further purification. Multi-walled CNTs (outer diameter < 8 nm, lengths 10-30 μm) were purchased from Chengdu Organic Chemicals. High-resolution transmission electron microscope (HRTEM) analysis showed that the average inner diameter of CNTs was around 3.9 nm and the wall thickness of it was in the range of 1.5-3 nm. Raw CNTs were refluxed in HNO_3 (68 wt.%) for 14 h at 140 °C in an oil bath to purify and cut the carbon tubes, in contrast, CNTs with closed caps were obtained by refluxing CNTs in 37 wt.% HNO_3 for 5 h at 100 °C. Then, the mixture was filtered and washed with deionized water, followed by drying at 60 °C for 12 h. HRTEM analysis indicated that the ends of the CNTs were open and the lengths of them were 0.5-2 μm.

Synthesis of Cu/Co-based catalysts

The CNTs were immersed in an ethanolic solution of precursor salts of Cu, Co and then subjected to ultrasonic treatment and stirring. The ultrasonic treatment and stirring facilitated the filling of the CNT channels with the precursor solution during impregnation. After 10 h of impregnation, the mixture was dried at 60 °C overnight, followed by heating to 110 °C for 10 h. This process afforded a homogeneous distribution of the active components inside the channels of the CNTs. After drying, the products were calcined in N_2 at 673 K for 4 h with a heating rate of 2 K min^{-1}. A series of catalysts were prepared using this method, i.e., 15Co/CNTs, 12.5Co2.5Cu /CNTs, 10Co5Cu/CNTs, 7.5Cu7.5Co/CNTs, 10Cu5Co/CNTs, 12.5Cu2.5Co/CNTs, 15Cu/CNTs, and the active components supported on CNTs with closed caps was denoted as 10Cu5Co-out-CNTs. These numbers stand for the loading metals weight contents.

Characterization

Powder X-ray diffraction patterns (XRD) were recorded over the 2θ range from 5 to 85° using a Rigaku MiniFlex II X-ray diffractometer, which was operated at 40 kV and 40 mA with Cu Kα radiation (k = 0.15418 nm) .

H_2-temperature-programmed reduction mass spectrometry analysis (H_2-TPR-MS) was performed to investigate the reducibility of the catalysts using a chemisorption instrument (TP-5080) and the sweep gas was detected using an OmniStar instrument. The catalyst (50 mg) was pre-treated at 300 °C under a flow of N_2 (32 mL min^{-1}) for 1 h and then cooled to 50 °C; after cooling, the flow was changed to a H_2/N_2 = 0.09 mixture (35 mL min^{-1}). The temperature-programmed reduction was performed between 50 and 800 °C with a heating rate of 10 °C min^{-1}.

X-ray photoelectron spectroscopy (XPS) and X-ray Auger electron spectroscopy (XAES) were used to analyze the change in the surface composition using an AXIS ULTRA DLD instrument equipped with Al Kα (hv = 1486.6 eV). The sample was reduced *in situ* under a flow of H_2 at 400 °C for 1 h, and the following photoelectron lines were recorded: Cu 2p, Co 2p, C 1s and O 1s. The binding energy values were corrected for charging effects by referring to the adventitious C1s line at 284.5 eV.

The chemical compositions (Cu and Co) of the as-prepared samples were determined by inductively coupled plasma-atomic emission spectroscopy (ICP-AES) using a Thermo iCAP 6300 instrument.

The textural properties of catalysts were measured by using the N_2-sorption isotherm at 77 K on a Micromeritics

ASAP2020 analyzer. Prior to each measurement, the sample was degassed at 200 °C overnight. The specific surface area was calculated by using the Brunauer-Emmett-Teller (BET) equation. The micropore volume was obtained from the t-plot method. The mesopore volume was obtained from the Barrett-Joyner-Halenda (BJH) method using the desorption branch. The pore size distributions were evaluated by using the density functional theory (DFT) method applied to the nitrogen adsorption data.

The morphologies and microstructures of the materials were observed using a high-resolution transmission electron microscope (JEOL, JEM-2100F), which was operated at 200 kV, with a lattice resolution of 0.14 nm.

Catalysis studies

Carbon monoxide hydrogenation reactions were performed in a 0.5 L continuous slurry reactor equipped with a mechanical agitator. The reactions were conducted at a temperature of 573 K and pressure of 4.5 MPa, using a feed gas of a 2:1 mixture of H_2 and CO at a space velocity of 10000 mL g_{cat}^{-1} h^{-1}. The catalysts were reduced with a 10% hydrogen-in-nitrogen mixture for 3 h at 673 K in a tube furnace. After cooling to room temperature under a flow of high purity nitrogen, the reduced catalysts were added into an agate mortar with liquid paraffin, the solid particles were finely powdered, then the mixed liquid paraffin were transferred into the slurry reactor. All experimental data were obtained under steady-state conditions that were invariably maintained for 7 h and no deactivation was observed. The products were analyzed using five online gas chromatographs (GCs) during the reaction. The organic gas products, consisting of hydrocarbons and methanol, were detected online by flame ionization measurements using a GC4000A (GDX-403 column). The long chain hydrocarbons in the oil phase were detected by flame ionization measurements using a GC-2010 (Rtx-1 capillary column). The inorganic gas products were detected online by thermal conductivity measurements using a GC4000A (carbon molecular sieves column). The H_2O and methanol products in the liquid phase were detected by thermal conductivity measurements using a GC4000A (GDX-401 column). The alcohol products in the liquid phase were detected by flame ionization measurements using a GC-7AG (Chromosorb 101).

Results and Discussion

Structural and morphological study of the catalysts

Figure 1 presents the XRD patterns of the fresh catalyst samples. As shown, the characteristic CNTs peak

was observed at a 2θ value of 25.8° and the intensity of peaks decreased gradually as a function of increased cobalt loading. The 15Cu/CNTs catalyst primarily consisted of a Cu_2O phase, with corresponding 2θ peak reflections positioned at 36.5, 42.4, 61.5, 73.7 and 77.6° (JCPDS No. 65-3288). Additionally, the CuO phase was also present in both the 15Cu/CNTs and 12.5Cu2.5Co/CNTs samples. As observed, the diffraction peak intensity of the CuO and Cu_2O species decreased gradually as the loading of Cu decreased. Furthermore, when the Co loading exceeded that of Cu, peaks corresponding to CoO (JCPDS No. 65-5474) were observed at very low intensities in these samples. In addition, carbon nanotubes seem to stabilize the CoO phase, which is usually unstable under ambient conditions. No other XRD characteristic peaks and significant shift of peaks were observed in these patterns, as bulk CoCu alloy may not be formed in the catalysts, due to the low solubility between Co and Cu. Furthermore, $CuCo_2O_4$ spinel or $Cu^{2+}_xCo^{2+}_{1-x}Co^{3+}_2O_4$ structure may also not exist in these samples because of the absence of Co_3O_4 phase.[25]
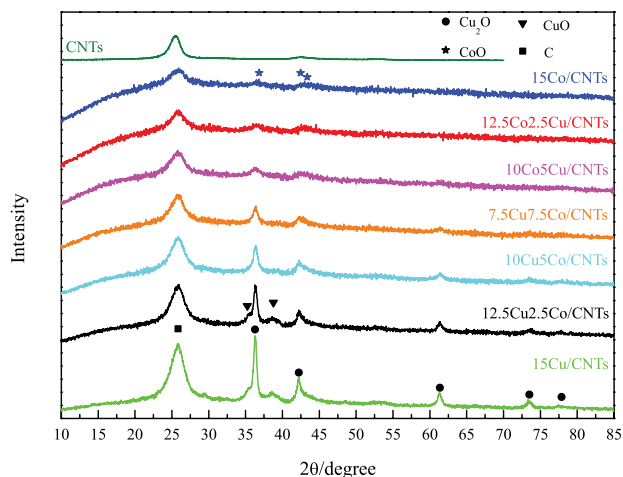

Figure 1. XRD patterns of the fresh catalysts.

The HRTEM images (Figures 2a-c) show nanoscale rows of metal particles in close proximity to each. As observed, the distances between two adjacent planes, d, were measured to be 0.24 and 0.21 nm, which are characteristic of Cu_2O and CoO phases, respectively. It is expected that such intimate contact among the metal particles would greatly improve the synergism of the Cu–Co dual sites and reduce side reactions. More HRTEM images are shown in Supplementary Information section (Figure S2), which could analyze the distribution of metal particles clearly. Additionally, approximately 81% of the particles reside within the channels of the 10Co5Cu/CNTs. In contrast, as shown in Figure 2e, 100% of the particles were located on

the exterior surface of 10Cu5Co-out-CNTs. Furthermore, the particle size distribution of the 10Co5Cu/CNTs catalyst (Figure 2c), shows a size distribution of 2-4 nm both inside and outside the nanotubes. However, the main particles size increased to 10-20 nm for 10Cu5Co-out-CNTs. After reaction, as shown in Figures 2d-f, grain growth of nanoparticles were found in the samples. The most abundant particles were in the size range of 2-30 nm for 10Co5Cu/CNTs and 10-40 nm for 10Cu5Co-out-CNTs. It is also observed that many particles still encapsulated within the channels of 10Co5Cu/CNTs after reaction. Therefore, the confinement effect of carbon nanotubes may considerably influence the distribution of metal particles, without the confinement effect of the tubes, the cobalt and copper particles are easily aggregated during the reaction.

The N_2-physisorption isotherms of the 10Co5Cu/CNTs catalyst are shown in Figure 3. According to the IUPAC classification, the catalyst exhibits a type IV isotherm having an inflection point around $P/P_0 = 0.4$. The BJH model was used to estimate mesopore size distributions. As shown in Figures 3a-b, it is observed that these samples possessed two types of mesopores, the CNT channels present a narrow pore size distribution with a pronounced peak at 3.4 nm, while the less uniform mesopores in the range of 10-50 nm were assigned to the interstitial voids among the CNTs. The BET surface area of the 10Co5Ce/CNTs and CNTs samples were 226 and 248 m^2 g^{-1}, respectively. It is indicated that all the samples has the similar BET surface area and pore size distribution.
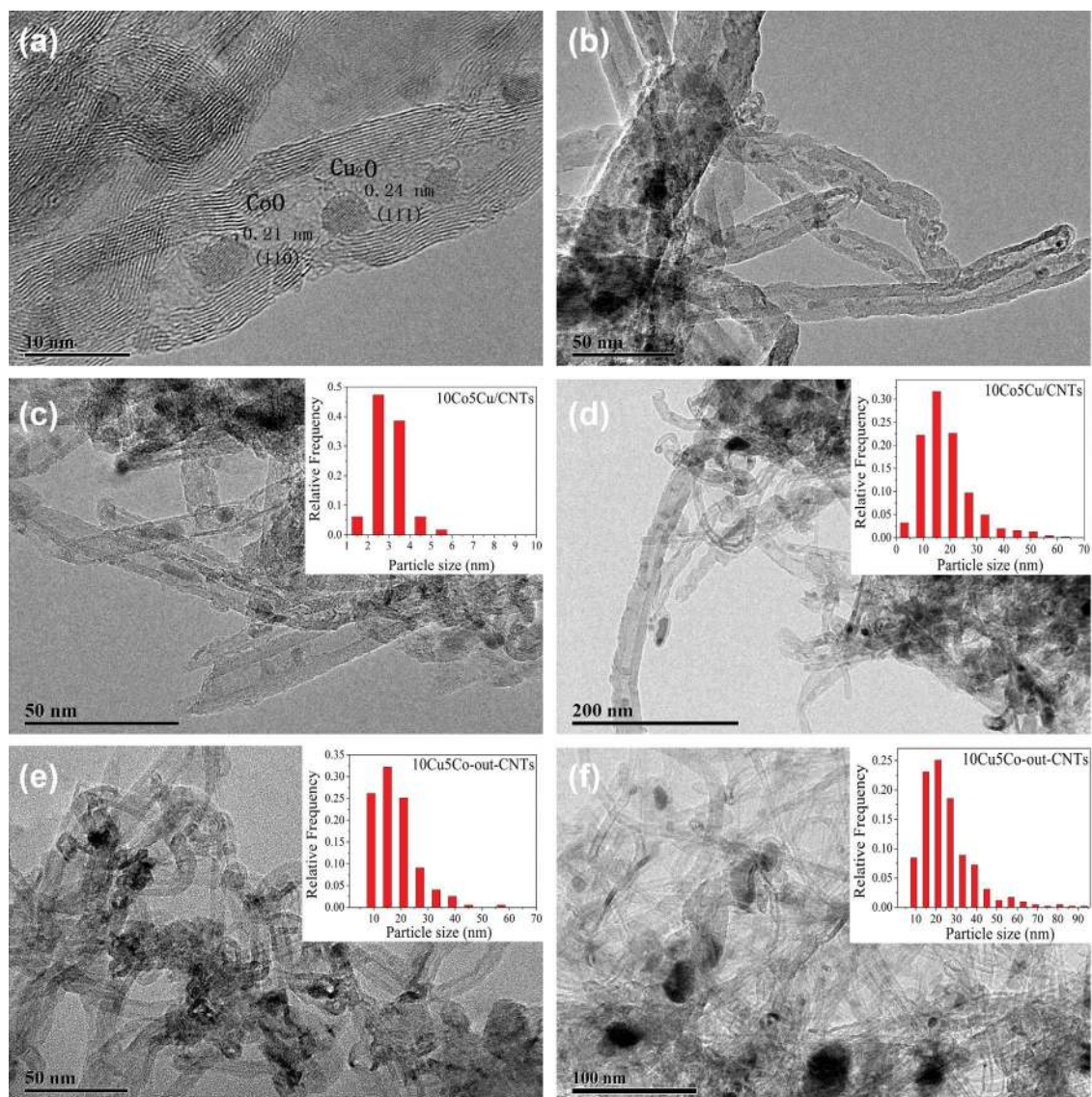

Figure 2. HRTEM images of fresh (a) 10Cu5Co/CNTs; (b) 7.5Cu7.5Co/CNTs; (c) 10Co5Cu/CNTs catalyst; (e) 10Cu5Co-out-CNTs; HRTEM images of used (d) 10Co5Cu/CNTs; (f) 10Cu5Co-out-CNTs, (600-700 particles were counted to determine the particle size distribution, and 300-400 particles were counted to calculate the percentage of particles inside and outside of the tubes).
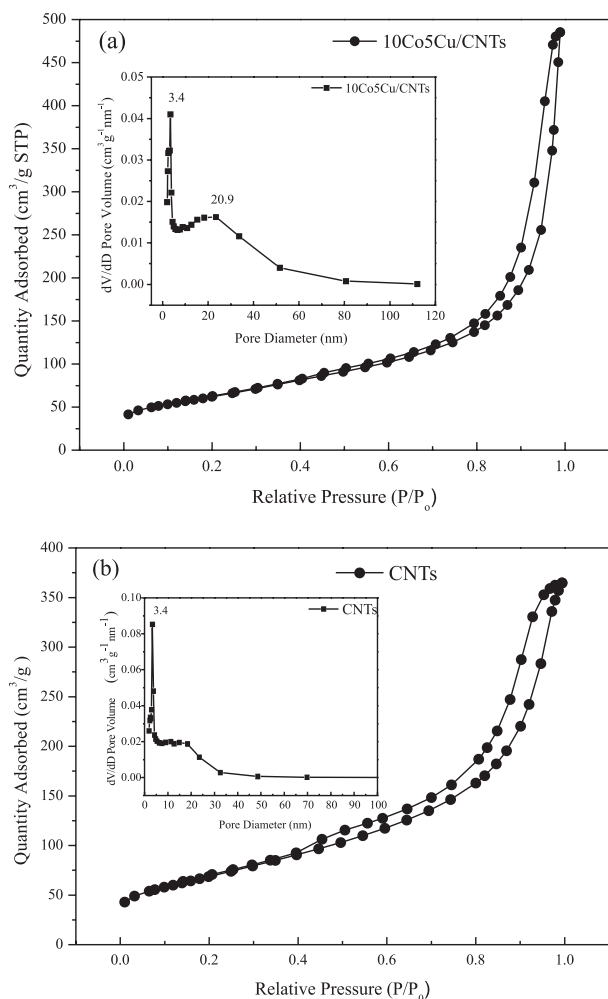
Figure 3. Nitrogen adsorption-desorption isotherms and pore size distributions of (a) the fresh 10Co5Cu/CNTs catalyst and (b) CNTs sample.

Catalytic performance evaluation

The catalytic performance of the CuCo/CNTs series of catalysts was studied and compared. The data is presented in Table 1. As observed, the 15Cu/CNTs catalyst

exhibited low activity and presented considerably low CO conversion and STY. Furthermore, methanol is the major product across alcohols formation. Conversely, the 12.5Cu2.5Co/CNTs catalyst exhibited considerably higher catalytic performance. The CO conversion and total alcohol STY increased by one order of magnitude relative to that of the 15Cu/CNTs sample. This result indicates that the addition of cobalt, even at low loading levels, has great influence on the properties of copper, and that there are synergistic effects between them. Additionally, the alcohol distribution results indicate that the reaction over CuCo/CNTs tends to favor the formation of C_{2+} alcohols. Thus, both structural and electronic interactions may exist between copper and cobalt.

As observed, the 7.5Cu7.5Co/CNTs catalyst displayed high activity and the selectivity of ethanol reached up to ca. 30.1%, with the selectivity for C_{2+} alcohols reaching ca. 57.7%. The 10Co5Cu/CNTs catalyst displayed a larger STY (372.9 mg g_{cat}^{-1} h^{-1}), together with a comparable higher alcohols distribution to that of the 10Cu5Co/CNTs sample. The 15Co/CNTs catalyst had a considerably higher activity with a CO conversion of 48.8% and a corresponding total alcohol selectivity of 13.4%. Further observations show that the selectivity for alcohols decreased as a function of increased cobalt loading in the catalysts. The excellent C_{2+} alcohols selectivity and yield are obtained over the catalyst with weight ratio of Cu/Co = 0.5-2. Taking high C_{2+} alcohols selectivity, low CO_2 selectivity and narrowed alcohols distribution into consideration, carbon nanotube-supported copper-cobalt catalyst turns to be better than CuZnAl[26] and Cu-Co/Mn_2O_3-Al_2O_3[27] catalyst recently reported for higher alcohols synthesis.

It is also observed that 10Cu5Co-out-CNTs exhibited a remarkably lower catalytic performance than that of 10Cu5Co/CNTs. The total alcohol STY decreased by 163.3 mg g_{cat}^{-1} h^{-1}, and furthermore, the total alcohols selectivity and the alcohol distribution results showed

Table 1. Catalytic performances of CuCo-based catalysts in CO hydrogenation

Sample	CO conversion / %	Total alcohol STY / (mg g_{cat}^{-1} h^{-1})	Carbon selectivity / (C mol%)				Alcohol distribution / (C mol%)				
			CH_4	C_2-C_4	ROH	CO_2	MeOH	EtOH	PrOH	BuOH	C_5OH
15Co/CNTs	48.8	256.5	68.5	9.1	13.4	9.0	59.2	25.1	10.1	5.2	0.4
12.5Co2.5Cu/CNTs	40.1	266.9	61.1	12.1	24.5	2.3	56.8	25.0	10.6	7.1	0.5
10Co5Cu/CNTs	38.9	372.9	48.5	14.0	35.8	1.7	52.7	26.5	12.5	7.3	1.1
7.5Cu7.5Co/CNTs	32.6	318.2	43.2	20.4	34.2	2.2	42.3	30.1	16.8	9.6	1.3
10Cu5Co/CNTs	28.9	292.3	44.9	17.6	36.3	1.2	50.0	28.0	13.0	7.8	1.2
12.5Cu2.5Co/CNTs	21.3	230.9	50.4	11.1	37.0	1.5	57.8	25.0	11.0	5.5	0.7
15Cu/CNTs	3.5	21.4	30.3	29.7	27.1	12.9	85.1	9.1	4.0	1.8	0.1
10Cu5Co-out-CNTs	14.0	129.0	60.7	8.7	28.6	2.0	60.2	23.6	10.9	4.9	0.5
CNTs	0	0	–	–	–	–	–	–	–	–	–

Reaction conditions: slurry reactor, 300 °C, 4.5 MPa, 10000 mL g_{cat}^{-1} h^{-1}, 2:1 H_2:CO syngas ratio, TOS: 7 h; STY: space-time yield; CNT: carbon nanotube.

that particles on the outside were not as effective for HAS as particles inside the CNTs. In addition, the pure CNTs sample exhibited no activity for higher alcohols synthesis through CO hydrogenation.

Correlation studies on the active sites and catalytic behavior

H$_2$-TPR characterization

The H$_2$-TPR profiles of the fresh catalysts are presented in Figure 4. Specifically, the 15Cu/CNTs sample exhibited a broad peak within the temperature range of 200 to 380 °C, which was attributed to the reduction of Cu$_2$O and CuO based on the XRD results. The 15Co/CNTs sample exhibited peaks centered at 292, 395 and 520 °C, which were primarily attributed to the reduction of CoO based on the XRD results. It was observed that the temperature of the first reduction peak decreased gradually as a function of increasing the Cu loading. Catalyst reduction is indicated to be influenced by the strong mutual effect of cobalt and copper, and the reduction of cobalt is considerably enhanced by the presence of copper, which results in an obvious enhancement of catalyst reducibility in our system. The similar conclusion was also proposed by other researchers.[28,29] Hence, the first broad peak in the CoCu/CNTs samples was attributed to the reduction of copper and cobaltous oxide. Additionally, a broad peak at ca. 480 °C was observed in all of these samples. To confirm the assignment of the broad peaks, TPR-mass spectrometry analysis was conducted and the results are shown in Supplementary Information section (Figure S1). It was found that a degree of cobaltous oxide was reduced at the higher temperatures, the addition of metals and metal oxides accelerated the decomposition of the nanotubes and their reduction peaks overlapped with the decomposition peak of the CNTs.
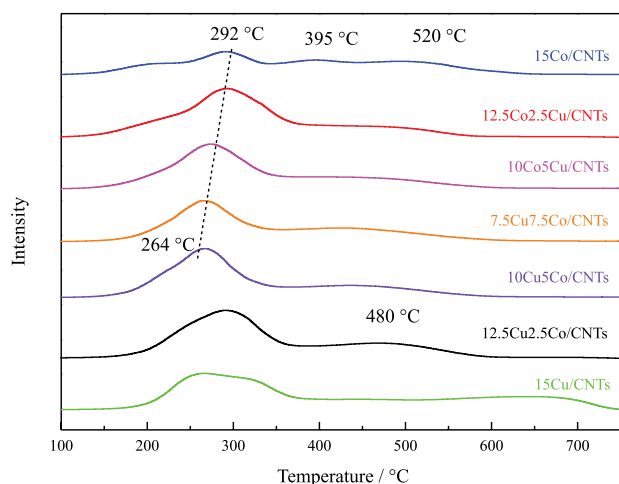

Figure 4. H$_2$-TPR profiles of the fresh catalysts.

XPS characterization

XPS is typically employed to analyze the composition and oxidation states of catalyst surface species. Thus, *in situ* and *ex situ* XPS spectra of the Cu 2p, Co 2p, C 1s and O 1s core levels of the 10Co5Cu/CNTs and 15Co/CNTs samples were recorded.

The Co 2p XPS spectra of the fresh and reduced 10Co5Cu/CNTs samples are shown in Figure 5a. The Co 2p$_{3/2}$ main peak was observed at ca. 780.7 eV, along with a satellite peak at 786.7 eV. The peak with the lowest binding energy (778.8 eV) is attributed to Co^0, whereas the peak observed at the higher binding energy (780.7 eV) is associated with Co^{2+} and the peak at 780.0 eV attributed to the Co^{3+} state.[30-32] To confirm the distribution of the Co species, the Co 2p XPS spectrum of the reduced 15Co/CNTs sample was measured (Figure 5c). The measured XPS surface layer revealed relative Co^0/(Co^0 + Co^{2+}) ratios in the reduced 10Co5Cu/CNTs and 15Co/CNTs catalysts of 2.92 and 3.61%, respectively. Based on the experimental results, the Co^{2+} site is thought to be beneficial for high alcohol selectivity, associatively adsorption of CO on Co^{2+} site and coupling of CO and CH$_x$ to form oxygenates. Similar results and discussion were also proposed by Wang *et al.*[33]

As shown in Figure 5b, the Cu 2p$_{3/2}$ spectrum of the fresh sample is characterized by a main peak at 932.69 eV with a satellite peak appearing at a higher binding energy, indicating the presence of surface Cu^{2+}.[34] Conversely, the Cu 2p$_{3/2}$ spectrum of the reduced sample was characterized by symmetrical major peaks and the absence of satellite structures. As XPS and XAES data show, for the fresh sample, E$_b$(Cu2p$_{3/2}$) is located at 932.69 eV with an E$_k$(CuL$_3$VV) value of 916.38 eV, giving an Auger parameter α′(Cu), of 1849.07 eV, which is associated with Cu$^+$. However, for the reduced sample, E$_b$(Cu2p$_{3/2}$) and E$_k$(CuL$_3$VV) values are 932.89 and 918.02 eV, respectively, giving an α′(Cu) of 1850.91 eV, which is associated with Cu^0.[35] Therefore, it could be deduced that only metallic copper is present on the surface of the catalysts after *in situ* reduction.

Compositional analysis to obtain Cu and Co content of the bulk 10Co5Cu/CNTs, 7.5Cu7.5Co/CNTs and 10Cu5Co/CNTs samples is measured using inductively coupled plasma-atomic emission spectroscopy (ICP-AES) and data is presented in Supplementary Information section (Table S1). Actual metal content reveals incorporation in ratios consistent with theoretical loading values.

Combined with the characterization analysis and experimental results, two mechanistic pathways are assumed for the CoCu-based catalysts in relation to the oxygenation of the generated carbon chain to form
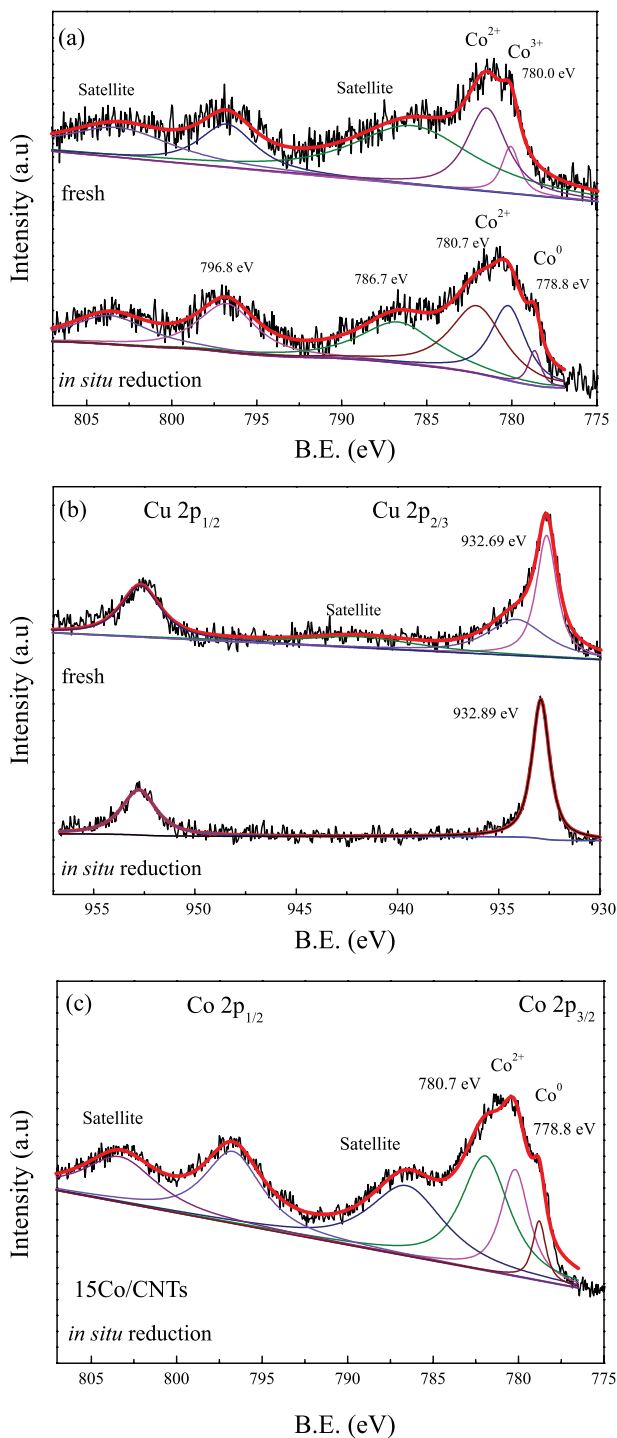
Figure 5. (a), (c) Co 2p and (b) Cu 2p XPS spectra of the fresh and reduced catalysts (*in situ* reduction was conducted in H_2 at 673 K for 1 h).

alcohols. The first route is a Cu^0–Co^0 center, with Co^0 acting as an active site for CO dissociation, C–C chain growth, and hydrogenation to produce $\cdot C_nH_x$ groups, whereas Cu^0 is the major site for methanol synthesis and is involved in the CO associative adsorption to form $CO\cdot$. The $CO\cdot$ moiety moves to the $\cdot C_nH_x$ group (or *vice versa*) and is inserted via surface migration

over a short distance between the Cu^0 and Co^0 sites for subsequent hydrogenation to produce higher carbon number alcohols. These alcohols synthesis mechanism has been termed as a CO insertion mechanism.[36] The second dual active site for alcohol synthesis is via the Co^0–Co^{2+} center, the surface reactions on these sites are similar to those on the Cu^0–Co^0 center. On the Co^0–Co^{2+} dual sites, metallic cobalt is the active site for CO dissociation and chain propagation, while Co^{2+} is the active site for CO associative adsorption and CO insertion, therefore Co^{2+} sites favor high oxygenate yields. A similar route for chain growth termination to produce alcohols was also proposed by Baker *et al.*[37] The metallic oxide Co pair (Co^0–Co^{2+}) could explain why the 15Co/CNTs sample also produces higher carbon number alcohols during the reaction; as shown in Table 1, the selectivity for total alcohol reaches up to 13.4%. The proposed mechanism is illustrated in Scheme 1.
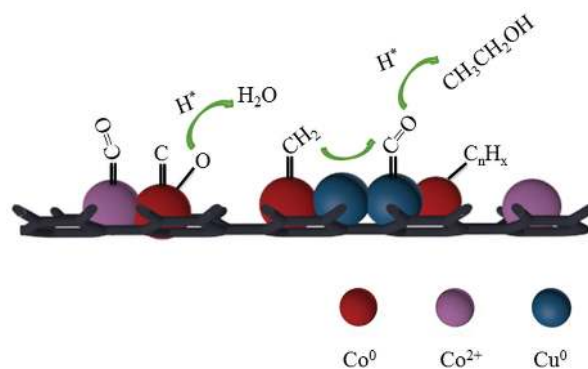
Scheme 1. Reaction model for the formation of higher alcohols over the CuCo/CNTs catalyst.

The Anderson-Schulz-Flory (ASF) plots (logarithm of mole fraction *vs*. carbon number) for the distribution of alcohols obtained over four catalysts are shown in Figure 6. The carbon number distributions of alcohols obtained over the 15Co/CNTs, 10Co5Cu/CNTs and 10Cu5Co/CNTs catalysts display excellent ASF plots. Partial deviation from the ASF distribution was observed for the 7.5Cu7.5Co/CNTs catalyst. The appropriate Cu/Co ratio enhances the synergistic effect of the active species and improves C_{2+} alcohol selectivity.

Conclusions

We have demonstrated that the bimetallic catalyst with a Cu/Co ratio from 0.5 to 2 favors higher carbon number alcohols formation during CO hydrogenation. The 7.5Cu7.5Co/CNTs catalyst exhibited a relatively high selectivity for the formation of ethanol (30.1%) and C_{2+} alcohols (57.7%) with a narrow range distribution, and
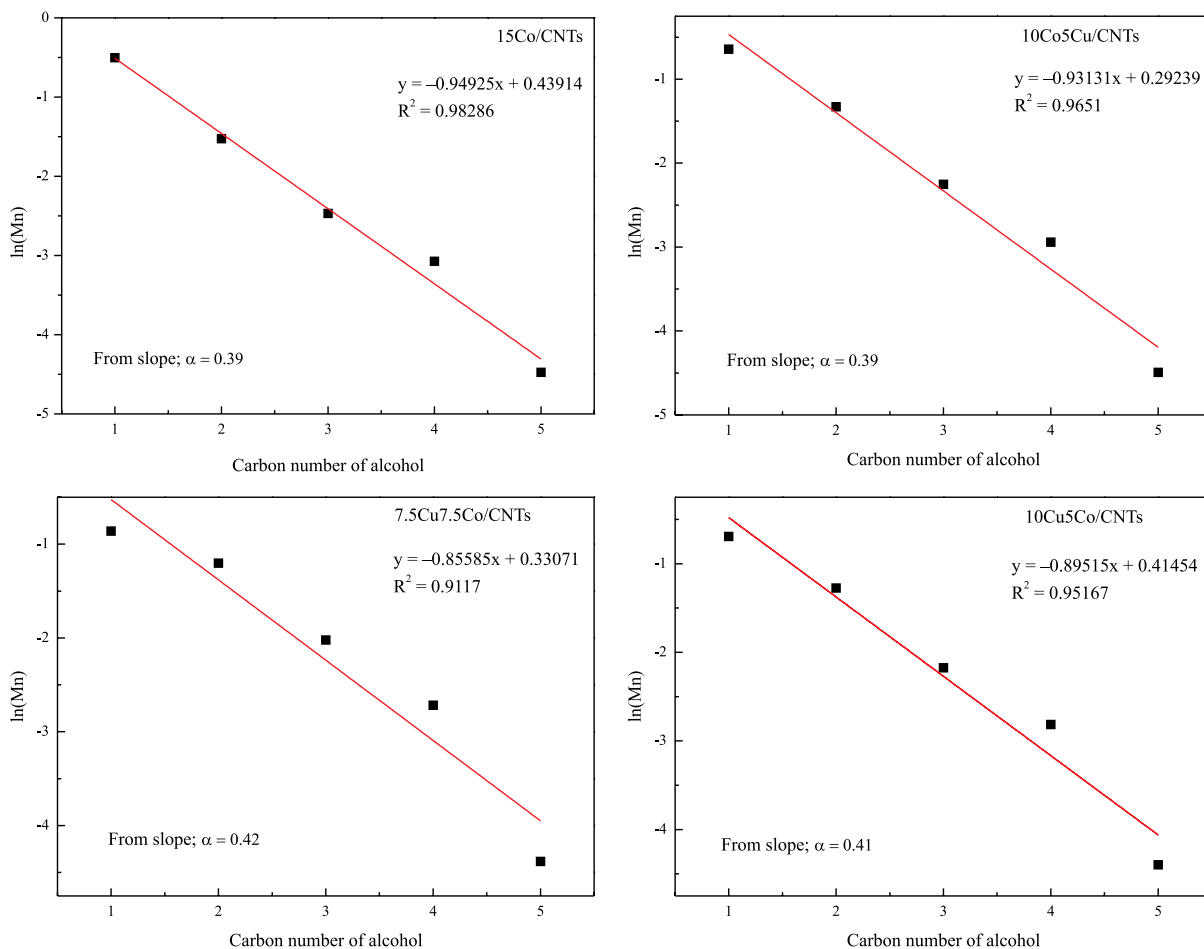
Figure 6. ASF plots for the distribution of alcohols obtained over the investigated catalysts.

the 10Co5Cu/CNTs catalyst displayed a high alcohol STY (372.9 mg g_{cat}^{-1} h^{-1}).

The superior confinement effect allows intimate contact between the copper-cobalt active species in the nanotubes, which improves their geometric interactions and synergistic effect. The synergistic effect between copper and cobalt is crucial for optimal product distribution. Metallic copper alone shows negligible catalytic activity for CO hydrogenation, however, in the presence of Cu^0–Co^0 dual catalytic sites, Cu is effective, as the sites for the oxygenation of the generated carbon chains form alcohols, in addition to enhancing cobalt reduction. Furthermore, the Co^0–Co^{2+} center is also beneficial to HAS, the Co^{2+} site terminating the carbon chain growth to produce alcohols and favor alcohols yields. The ratio of Cu/Co considerably influences metal particle properties and it likely plays an important role in determining the selectivity towards higher alcohols.

Supplementary Information

Supplementary data (H_2-TPR-MS, HRTEM and ICP

results) are available free of charge at http://jbcs.sbq.org.br as PDF file.

References

1. Luk, H. T.; Mondelli, C.; Ferré, D. C.; Pérez-Ramírez, J.; *Chem. Soc. Rev.* **2017**, *46*, 1358.

2. Gangwal, V.; Gangwal, S. K.; *Energy Fuels* **2008**, *22*, 814.

3. Wang, P.; Chen, S. Y.; Bai, Y. X.; Gao, X. F.; Sun, K.; Han, Y. Z.; Tan, Y. S.; *Fuel* **2017**, *195*, 69.

4. Gupta, M.; Smith, M. L.; Spivey, J. J.; *ACS Catal.* **2011**, *1*, 641.

5. Wang, J. J.; Chernavskii, P. A.; Khodakov, A. Y.; Wang, Y.; *J. Catal.* **2012**, *286*, 51.

6. Fang, K. G.; Li, D. B.; Lin, M. G.; Xiang, M. L.; Wei, W.; Sun, Y. H.; *Catal. Today* **2009**, *147*, 133.

7. Medford, A. J.; Lausche, A. C.; Temel, B.; Schjodt, N. C.; Norskov, J. K.; *Top. Catal.* **2014**, *57*, 135.

8. Prieto, G.; Beijer S.; Smith, M. L.; Au, Y.; Wang, Z.; *Angew. Chem., Int. Ed.* **2014**, *53*, 6397.

9. Xiaoding, X.; Doesburg, E. B. M.; Scholten, J. J. F.; *Catal. Today* **1987**, *2*, 125.

10. Smith, K. J.; Anderson, R. B.; *J. Catal.* **1984**, *85*, 428.

11. Xiao, K.; Bao, Z. H.; Fang, K. G.; Lin, M. G.; Sun, Y. H.; *Chin. J. Catal.* **2013**, *34*, 116.

12. Subramanian, N. D.; Balaji, G.; Kumar, C.; Spivey, J. J.; *Catal. Today* **2009**, *147*, 100.

13. Khodakov, A. Y.; Griboval-Constant, A.; Bechara, R.; Zholobenko, V. L.; *J. Catal.* **2002**, *206*, 230.

14. Borg, Ø.; Eri, S.; Blekkan, E. A.; Storsæter, S.; Wigum, H.; Rytter, E.; *J. Catal.* **2007**, *248*, 89.

15. Khodakov, A. Y.; Bechara, R.; Griboval-Constant, A.; *Appl. Catal., A* **2003**, *254*, 273.

16. Karaca, H.; Safonova, O. V.; Chambrey, S.; Fongarland, P.; Roussel, P.; *J. Catal.* **2011**, *277*, 14.

17. Karaca, H.; Hong, J.; Fongarland, P.; Roussel, P.; Lacroix, M.; *Chem. Commun.* **2010**, *46*, 788.

18. den Otter, J. H.; Nijveld, S. R.; de Jong, K. P.; *ACS Catal.* **2016**, *6*, 1616.

19. Deng, D.; Yu, L.; Chen, X.; Wang, G.; Jin, L.; Pan, X.; *Angew. Chem., Int. Ed.* **2013**, *52*, 371.

20. Chen, W.; Fan, Z.; Pan, X.; Bao, X.; *J. Am. Chem. Soc.* **2008**, *130*, 9414.

21. Chen, W.; Pan, X. L.; Willinger, M. G.; Su, D. S.; Bao, X. H.; *J. Am. Chem. Soc*. **2006**, *128*, 3136.

22. Pan, X.; Fan, Z.; Chen, W.; Ding, Y.; Luo, H.; Bao, X.; *Nat. Mater.* **2007**, *6*, 507.

23. Guan, J.; Pan, X. L.; Liu, X.; Bao, X. H.; *J. Phys. Chem. C* **2009**, *113*, 21687.

24. Guo, S.; Pan, X.; Gao, H.; Yang, Z.; Zhao, J.; Bao, X. H.; *Chem. - Eur. J.* **2010**, *16*, 5379.

25. Su, J.; Zhang, Z.; Fu, D.; Jiang, Z.; Xu, J.; Han, Y. F.; *J. Catal.* **2016**, *336*, 94.

26. Liu, Y.; Deng, X.; Han, P.; Huang, W.; *Fuel Process. Technol.* **2017**, *167*, 575.

27. Zhao, L.; Li, W.; Zhou, J.; Mu, X.; Fang, K.; *Int. J. Hydrogen Energy* **2017**, *421*, 7414.

28. Wang, J. J.; Chernavskii, P. A.; Khodakov, A.Y.; Wang, Y.; *J. Catal.* **2012**, *286*, 51.

29. Fierro, G.; Jacono, M. L.; Inversi, M.; Dragone, R.; Porta, P.; *Top. Catal.* **2000**, *10*, 39.

30. Reinikainen, M.; Niemelä, M. K.; Kakuta, N.; Suhonen, S.; *Appl. Catal., A* **1998**, *174*, 61.

31. Guczi, L.; Bazin, D.; Kovács, I.; Borkó, L.; Schay, Z.; Lynch, J.; *Top. Catal.* **2002**, *20*, 129.

32. Ernst, B.; Bensaddik, A.; Hilaire, L.; Chaumette, P.; Kiennemann, A.; *Catal. Today* **1998**, *39*, 329.

33. Wang, Z.; Kumar, N.; Spivey, J. J.; *J. Catal.* **2016**, *339*, 1.

34. Wang, J.; Chernavskii, P. A.; Wang, Y.; Khodakov, A. Y.; *Fuel* **2013**, *103*, 1111.

35. Wang, P.; Huang, W.; Zhang, G.; Gao, Z.; Tang, Y.; Sun, K.; *J. Ind. Eng. Chem.* **2015**, *26*, 243.

36. Fang, K.; Li, D.; Lin, M.; Xiang, M.; Wei, W.; Sun, Y.; *Catal. Today* **2009**, *147*, 133.

37. Baker, J. E.; Burch, R.; Hibble, S. J.; Loader, P. K.; *Appl. Catal.* **1990**, *65*, 281.